

An Introduction to the Evaluation of Spin Structure Functions from Experimental Data

R.Windmolders ¹.

Physikalisches Institut Universität Bonn, Nussallee 12 D-53115 Bonn, Germany

November 10, 2018

Abstract

These lectures introduce the non-specialist to the evaluation of spin structure functions from asymmetries measured in polarized deep-inelastic scattering experiments. The various steps leading from apparatus dependent counting rate asymmetries to physics asymmetries are described. Special attention is given to the effects of time variation in detector acceptances, to the use of deuterium as a neutron target and to the corrections due to the presence of unpolarized material in a polarized target. These topics are illustrated by examples taken from the CERN muon experiments.

Lectures given at the 10th "Séminaire Rhodanien de Physique" held at the Villa Gualino, Torino, March 4-8, 2002.

¹Supported by the Bundesministerium für Bildung und Forschung, contract Nr 06BN908I

1 Introduction.

In these lectures we discuss experimental problems arising in the evaluation of the nucleon spin structure from data taken in high energy polarized lepton-nucleon scattering experiments.

A general introduction to the formalism of nucleon spin structure functions as well as their interpretation in terms of constituents can be found in recent textbooks on particle physics [1]. Only a short overview will be presented here in order to define the kinematic variables and to introduce the relevant physics parameters. Spin structure functions are measured in experiments performed with incident electron or muon beams. These experiments are called "inclusive" because only the incident and scattered lepton are measured:

$$\ell N \rightarrow \ell' X. \quad (1)$$

The symbol X represents the unmeasured hadron final state which generally consists of several particles. The kinematics of the reaction is entirely determined by 2 variables ν and Q^2 which, in the lab system, are respectively the energy of the exchanged virtual photon and minus the square of its mass (Fig. 1):

$$\begin{aligned} \nu &= k_0 - k'_0 \\ Q^2 &= -q^2 = (\bar{k} - \bar{k}')^2 - (k_0 - k'_0)^2. \end{aligned} \quad (2)$$

In these lectures, we will consider only the region of deep inelastic scattering ("DIS"), where the mass of the hadron system X is much larger than the proton mass. This condition is equivalent to requiring sufficiently large values of ν and Q^2 . We also assume that the exchange of a virtual photon is the only process contributing significantly to the reaction, which means that weak interactions mediated by the exchange of a Z^0 or W gauge boson are negligible. In practice, the latter condition is satisfied for all fixed target experiments.

The main feature of lepton scattering in the DIS region is the **approximate scaling of the differential cross sections**: for sufficiently large values of ν and Q^2 , the cross section only depends on the scaling variable defined by

$$x = \frac{Q^2}{2M\nu} \quad (3)$$

where M is the nucleon mass. The discovery of scaling in 1967 has given an experimental basis to the quark model. Scaling means that, at fixed x , the cross section does not depend on the value of Q^2 or, in other words, on the size of the probed object. Scaling therefore suggests that the scattering must take place on pointlike constituents ("partons") of the nucleon. In the quark-parton model, the scaling variable x is equal to the fraction of the nucleon momentum carried by the quark which has absorbed the virtual photon.

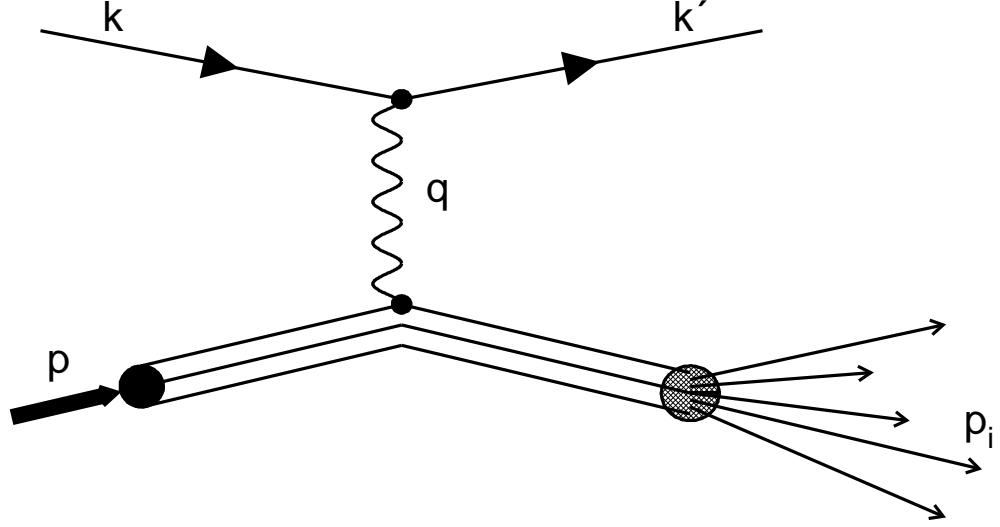


Figure 1: *Deep inelastic scattering of a lepton with four-momentum k on a nucleon with four-momentum p resulting into a lepton with four-momentum k' and a hadronic system.*

Spin effects generate a difference between the cross sections for parallel and antiparallel orientations of the beam and target spins $\sigma^{\leftarrow\leftarrow}$ and $\sigma^{\leftarrow\Rightarrow}$. In order to discuss these effects, we introduce the **spin averaged cross section**

$$\bar{\sigma} = \frac{1}{2}(\sigma^{\leftarrow\Rightarrow} + \sigma^{\leftarrow\leftarrow}) \quad (4)$$

which is measured in unpolarized experiments, and the **spin dependent cross section**

$$\Delta\sigma = (\sigma^{\leftarrow\Rightarrow} - \sigma^{\leftarrow\leftarrow}), \quad (5)$$

which can only be measured in experiments where beam and target are both polarized. In the deep inelastic region, the differential cross sections are expressed in terms of two **structure functions** which depend mainly on the scaling variable x and, because scaling is only approximate, to a smaller extent on Q^2 :

$$\begin{aligned} d^2\bar{\sigma}/(dx dQ^2) &= a F_1(x, Q^2) + b F_2(x, Q^2) \\ d^2\Delta\sigma/(dx dQ^2) &= c g_1(x, Q^2) + d g_2(x, Q^2). \end{aligned} \quad (6)$$

The unpolarized structure functions F_1 and F_2 are related in the quark-parton model by the Callan-Gross relation

$$2 x F_1(x) = F_2(x) \quad (7)$$

and more generally by the relation ²

$$F_1(x, Q^2) \cong \frac{F_2(x, Q^2)}{2x(1 + R(x, Q^2))} \quad (8)$$

where $R(x, Q^2)$ is found to be small. The Q^2 dependence of the structure functions ("scaling violation") is due to interactions between nucleon constituents and is successfully described in the context of quantum chromodynamics ("QCD").

The second structure function $g_2(x, Q^2)$ has been found to be small. For the longitudinal spin configuration which is discussed here, its contribution is further suppressed due to the small value of the coefficient d and can safely be neglected. The **cross section asymmetry** defined by

$$A_{\parallel} = \frac{\Delta\sigma}{2\bar{\sigma}} \quad (9)$$

can then be written as

$$A_{\parallel} \cong D \frac{g_1(x, Q^2)}{F_1(x, Q^2)} \quad (10)$$

where the coefficient D is directly calculable from the kinematic factors a , b and c of Eqn.(6). The evaluation of the asymmetry A_{\parallel} , which is the main purpose of most experiments in polarized DIS, gives access to the spin structure function g_1 using the spin averaged functions F_1 or F_2 known from unpolarized experiments. The remaining part of these lectures will describe the various steps involved in the derivation of A_{\parallel} from experimental data with special emphasis on some problems specific to muon experiments.

At the constituent level, spin effects in DIS can be intuitively understood by the fact that a quark having its spin projection along the reference axis (+OZ) can absorb a virtual photon which has its spin projection along (-OZ) and flip its spin, while no absorption can occur when the two spins in the initial state are oriented in the same direction.

Defining $q_i^+(x)$ and $q_i^-(x)$ as the distributions of quarks of flavor i with spin along or opposite the nucleon spin, we see that the absorption cross section for virtual photons with spin projection opposite to the nucleon spin ($\sigma_{1/2}$) will be proportionnal to q_i^+ while the absorption cross section for virtual photons with spin parallel to the nucleon spin ($\sigma_{3/2}$) will be proportionnal to q_i^- . The **virtual photon asymmetry** is obtained by summing over the quark flavors i and multiplying each term by the square of the quark charge expressed in units of the electron charge ($e_i^2 = 4/9$ or $1/9$):

$$A_1 = \frac{\sigma_{1/2} - \sigma_{3/2}}{\sigma_{1/2} + \sigma_{3/2}} \cong \frac{\sum e_i^2 (q_i^+(x) - q_i^-(x))}{\sum e_i^2 (q_i^+(x) + q_i^-(x))}. \quad (11)$$

The denominator in the previous expression shows the well known decomposition of F_1 in terms of quark flavors. The numerator provides the corresponding decomposition of g_1 in terms of the quark spin distributions $\Delta q_i(x) = q_i^+(x) - q_i^-(x)$. Comparing with

² The symbol \cong is used in Eqns.(8-11) to warn the reader that a kinematic factor close to 1.0 for $\nu^2 \gg Q^2$ has been neglected.

the definition of A_{\parallel} given in Eqn.(10), we see that the factor D can be considered as the depolarization of the virtual photon. This factor depends mainly on the fraction $y = \nu/k_0$ of the beam energy taken away by the virtual photon and is close to 1 for virtual photons carrying nearly the total energy of the incoming leptons.

2 Polarized DIS experiments.

2.1 General characteristics of electron and muon experiments.

The first polarized DIS experiments have been performed at SLAC in the early 80's [2]. Experiments using polarized electron beams are presently running at JLAB (Virginia) in the energy range of 2-5 GeV [3], at SLAC [4] in the range of 10-50 GeV and at DESY at 27 GeV [5].

These experiments use high intensity beams (e.g. 10^{12} electrons per second at SLAC) and consequently need only relatively small targets to reach a high statistical accuracy. They can invert very frequently either the beam polarization (JLAB, SLAC) or the target polarization (DESY) and are therefore not very sensitive to systematic effects due to changes in detector acceptance. Their kinematic range is however limited due to the relatively low incident energy.

The muon experiments, mainly performed at CERN, have opposite characteristics: their energy range is much higher (100-200 GeV) and their beam intensity much lower (10^7 muons per second, i.e. down by a factor 10^5 compared to SLAC). The incident muons are obtained from 2 body decays of π 's and K 's and are naturally polarized due to the non-conservation of parity in the weak decay. Positively charged muons produced in a direction close to the primary hadron beam have a negative polarization of about 80 % [6].

Due to the limited intensity, muon experiments need large polarized targets. Furthermore, in order to limit systematic effects due to acceptance variation, it is essential to use simultaneously 2 target cells with opposite polarization and to invert the polarization at regular intervals. The SMC target [7] which has been in use at CERN since 1993 is shown as an exemple in Fig. 2 and will be described in a further section. Since the time interval between 2 consecutive reversals of the polarization is at least of the order of a few hours, the time dependence of detector acceptances becomes a critical issue in muon experiments.

2.2 Counting rates and cross sections.

If we consider 2 consecutive runs with beam and target polarization parallel and antiparallel and with incident lepton fluxes ϕ_1 and ϕ_2 respectively, the numbers of collected

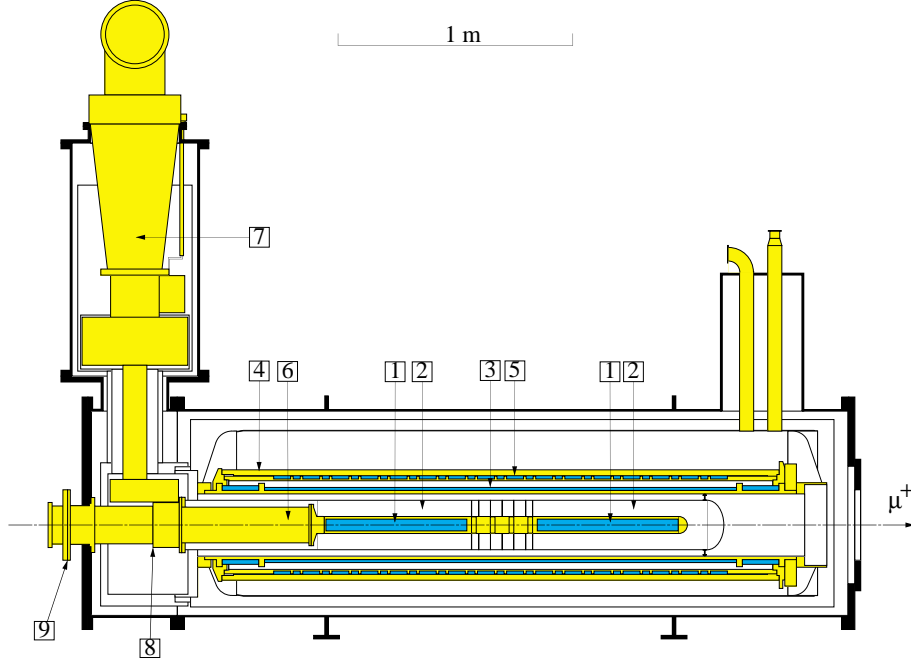


Figure 2: *The SMC target cryostat with the target holder as used since 1993. The muon beam traverses the cryostat from left to right. (1) target cells, (2) microwave cavity, (3) solenoid coil, (4) dipole coil, (5) correction coils, (6) dilution refrigerator, (7) precooler of ^3He , (8) indium seal, and (9) external seal.*

interactions (N_1, N_2) will be related to the cross sections (4-5) by the following formulas:

$$\begin{aligned} N_1 &= n \phi_1 a (\bar{\sigma} - (1/2)f P_b P_T \Delta\sigma) \\ N_2 &= n \phi_2 a (\bar{\sigma} + (1/2)f P_b P_T \Delta\sigma). \end{aligned} \quad (12)$$

Here n stands for the area density of target nucleons, a for the acceptance, f for the fraction of polarizable material in the target and P_b (P_T) for the beam (target) polarization. At first sight, it looks straightforward to extract $\Delta\sigma$ from these relations. However, one should keep in mind that the spin dependent term is about 1000 times smaller than the spin averaged one and that the large fluxes cannot be determined with a precision better than a few percent. In practice, the uncertainty on the fluxes totally masks the spin contribution and makes a direct determination of $\Delta\sigma$ impossible. As a consequence, spin experiments do not measure cross sections but asymmetries.

2.3 Counting rate asymmetries and spin asymmetries.

As an example we now consider 2 target cells of same density n with opposite polarization exposed to the same incident flux ϕ .

Under the unrealistic assumption that the spectrometer acceptance would be the same

for the 2 cells, the counting rate asymmetry

$$\delta = \frac{N_2 - N_1}{N_2 + N_1} \quad (13)$$

is obviously proportional to the cross section asymmetry defined by Eqn.(9):

$$\delta = f P_b P_T A_{\parallel}. \quad (14)$$

(We will see in the next section how the different acceptances for 2 target cells should be taken into account.)

The statistical error on δ

$$\sigma(\delta) = \frac{(4N_1N_2)^{1/2}}{(N_1 + N_2)^{3/2}} \quad (15)$$

reduces to $1/(N_1 + N_2)^{1/2}$ when the asymmetry is small. A large statistics will thus be required to reach a significant precision on a small asymmetry. For instance, if $\delta \simeq 10^{-4}$, a relative precision $\sigma(\delta)/\delta = 0.1$ corresponds to a 10^{10} interactions.

The statistical error on the physics asymmetry A_{\parallel} is further divided by the product $P_b P_T f$. It is thus essential to keep these 3 factors as large as possible: a reduction by a factor α must indeed be compensated by increasing the number of interactions N_{tot} by α^2 . As a consequence, the **figure of merit** for the comparison of experiments performed with different beams or different targets is given by

$$(P_b P_T f)^2 N_{tot}. \quad (16)$$

All published values of the spin structure function g_1 have been obtained from cross section asymmetries derived from counting rate asymmetries according to Eqn.(14). The relation between A_{\parallel} and g_1

$$g_1(x, Q^2) = \frac{A_{\parallel}(x, Q^2)}{D} \frac{F_2(x, Q^2)}{2 x (1 + R(x, Q^2))} \quad (17)$$

involves the use of parametrizations of the unpolarized structure functions F_2 and R based on a large number of measurements from many experiments. The uncertainty due to these parametrizations is included in the systematic error on g_1 . The statistical error on g_1 is propagated from the statistical error on A_{\parallel} and tends to increase at low x due to the presence of the factor x in the denominator. This effect is well visible on the 3 data set shown in Fig. 3. The difference between the g_1 values for experiment E143 with respect to the CERN experiments reflects the Q^2 dependence of the structure function: at any fixed x , the average Q^2 is about 6 times larger for the EMC-SMC data than for the E143 data. It can be observed that this difference in Q^2 generates a sizable scaling violation in the region $x < 0.10$. The curves on the figure show that this effect is well described in fits based on perturbative QCD [8].

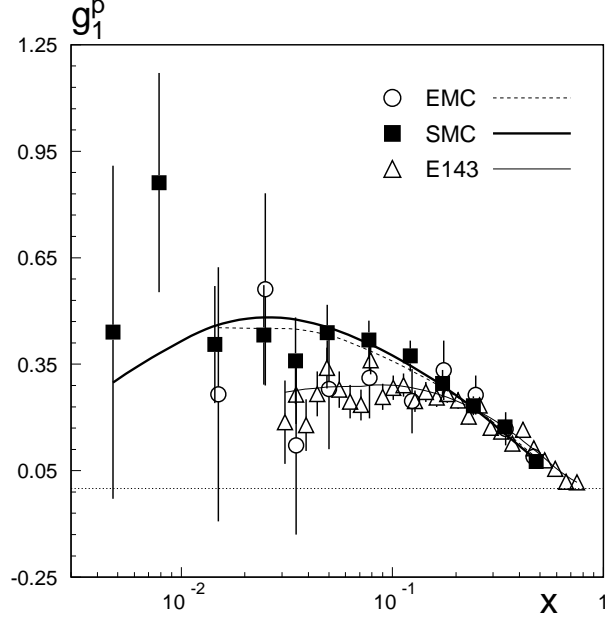


Figure 3: Three data sets on g_1^p . The curves show the QCD fit at the measured Q^2 of each data point. Error bars represent the total error.

2.4 Acceptance corrected counting rate asymmetries.

We now come to the realistic case where two target cells (labelled "u" (up) and "d" (down)) are exposed to incident fluxes ϕ and ϕ' in 2 consecutive runs [9]. In the first run, the "u" target polarization is opposite to the beam polarization while the "d" target polarization is directed along the beam polarization. In the second run, the polarizations of the 2 cells are reversed. Defining $m = P_b |P_T| f$, we obtain the following relations between numbers of events and cross sections:

$$\begin{aligned}
 N_u &= n_u \phi a_u \bar{\sigma} (1 + m A_{\parallel}), \\
 N_d &= n_d \phi a_d \bar{\sigma} (1 - m A_{\parallel}), \\
 N'_u &= n_u \phi' a'_u \bar{\sigma} (1 - m A_{\parallel}), \\
 N'_d &= n_d \phi' a'_d \bar{\sigma} (1 + m A_{\parallel}).
 \end{aligned} \tag{18}$$

The counting rate asymmetries for the configurations before and after polarization reversal are

$$\delta = \frac{N_u - N_d}{N_u + N_d}, \tag{19}$$

$$\delta' = \frac{N'_d - N'_u}{N'_d + N'_u}. \tag{20}$$

Eliminating the ratio $(n_d a_d)/(n_u a_u)$ between the 2 previous relations and defining the ratio of ratios of acceptance before and after reversal $K = (a'_d/a'_u)/(a_d/a_u)$, we obtain

$$\frac{(1 - mA_{\parallel})^2}{(1 + mA_{\parallel})^2} = K \frac{(1 - \delta)(1 - \delta')}{(1 + \delta)(1 + \delta')} \tag{21}$$

which is a second order equation in A_{\parallel} . Keeping the solution satisfying $|A_{\parallel}| \leq 1$ and approximating

$$\left((1 - \delta^2)(1 - \delta'^2)\right)^{1/2} \simeq 1 - (1/2) (\delta^2 + \delta'^2) \quad (22)$$

we obtain for the case where $K = 1$:

$$A_{\parallel} = \frac{\delta + \delta'}{2m}. \quad (23)$$

Under the condition that the ratio of acceptances for the 2 target cells remains unchanged after polarization reversal (i.e. $K = 1$), we thus obtain an unbiased estimate of the physics asymmetry by taking the arithmetic mean of the counting rate asymmetries before and after polarization reversal.

The derivation is slightly more complicated when K is different from 1 [10]. In this case, since K is nevertheless close to 1, one may expand $\sqrt{K} = \sqrt{1 + \epsilon} \simeq 1 + \epsilon/2 - \epsilon^2/8$ and drop all square terms multiplied by ϵ in Eqn.(21) which leads to

$$A_{\parallel} = \frac{(\delta + \delta')^2 - \epsilon(\delta + \delta') + \epsilon^2/4}{m(2(\delta + \delta') - \epsilon(1 - \delta - \delta'))}. \quad (24)$$

This in turn can be approximated by

$$A_{\parallel} = \frac{1}{m} \left(\frac{\delta + \delta'}{2} - \frac{\epsilon}{4} \right). \quad (25)$$

Here the first term correspond to the result obtained for the case $K = 1$. The second term is a **false asymmetry due to the change of the acceptance ratio**. We also observe that even a small deviation of K from the nominal value of 1 generates a sizable false asymmetry: in the case where $(\delta + \delta')/2 \simeq 0.01$, a value $K = 0.97$ results in a false asymmetry of the same order as the physics asymmetry and spoils the data. It is thus essential to keep track of all changes in acceptances which may affect the value of K and to eliminate data sets where the ratio of acceptances deviates significantly from its nominal value. The risk of such deviations obviously decreases when the frequency of polarization reversals increases. Electron experiments where the polarization can be inverted for each accelerator pulse are practically unaffected by this false asymmetry while muon experiments need to reduce the time between consecutive polarization reversals to the minimum acceptable.

3 Solid polarized targets.

Solid polarized targets, such as the one described in [7], are based on the alignment of spins in a magnetic field H . In paramagnetic materials, spins of free electrons align with the magnetic field which, at equilibrium, gives rise to a polarization

$$P = \frac{n_+ - n_-}{n_+ + n_-} = \tanh\left(\frac{\mu_B H}{k T}\right), \quad (26)$$

where μ_B is the Bohr magneton and k the Boltzmann constant. For a field of $2.5T$ and a temperature of $0.5 K$, this corresponds to a polarization of nearly 100 %. Similar considerations apply to the proton spin but result, with the same field and temperature, into a polarization of only 0.5 %. It is thus essential to apply a process transferring the electron polarization to the protons in order to obtain an usable polarized target.

Dynamic nuclear polarization ("DNP") fulfills this requirement and can be understood at the most basic level by considering a system composed of a non-interacting proton and electron in a magnetic field. The 4 energy levels $|s_e, s_p\rangle$ will be characterized by different projections of the electron spin (first label) or the proton spin (second label) on the direction of the magnetic field: $|-, +\rangle$, $|-, -\rangle$, $|+, +\rangle$ and $|+, -\rangle$ corresponding respectively to the energy levels E_a , E_b , E_c and E_d . The difference $E_c - E_a$ for opposite orientations of the electron spin corresponds to a frequency $\nu_e = 70$ Ghz while the difference for nucleon spin orientations $E_b - E_a$ corresponds to $\nu_N = 106$ Mhz. At equilibrium, the relative population is thus about 50 % for each of the 2 lowest levels while the 2 other ones are nearly empty.

If a radio frequency $\nu = \nu_e + \nu_N$ is applied, a fraction $\tilde{\epsilon}$ of the population of level a will be moved to level d . This will be followed by a spontaneous transition from level d to level b due to the strong coupling of the electron spins with the field and result into a proton polarization $P_N = 2 \tilde{\epsilon}$. The opposite effect would be obtained by applying a radio frequency $\nu = \nu_e - \nu_N$.

DNP can only take place when several conditions are fulfilled: presence of the right amount of paramagnetic centers in the material, a field strong enough to reach the appropriate separation of energy levels and a temperature low enough to keep the width of these levels small. Under optimal conditions, values of the proton polarization comparable to the electron polarization can be reached.

Fig. 4 shows the polarization build-up for the various materials used in the SMC experiment [7]. About 10 hours are needed before the polarization becomes close to its maximum level. Changing the polarization by changing the radio-frequency is thus a time consuming process which can only take place during a long interruption of the data taking. More frequent polarization reversals are obtained by the so-called "field rotation": the polarization is maintained by a transverse field of 0.5 T produced by a dipole coil (Fig. 2) while the solenoid field is ramped down and brought back in the opposite direction in a process requiring less than half an hour.

4 Deuterium as a neutron target.

The difference of the spin structure functions g_1 for the proton and the neutron is one of the key issues in polarized DIS [8]. While proton data are obtained directly from hydrogen targets, neutron data must be extracted from data taken on a deuterium or helium target.

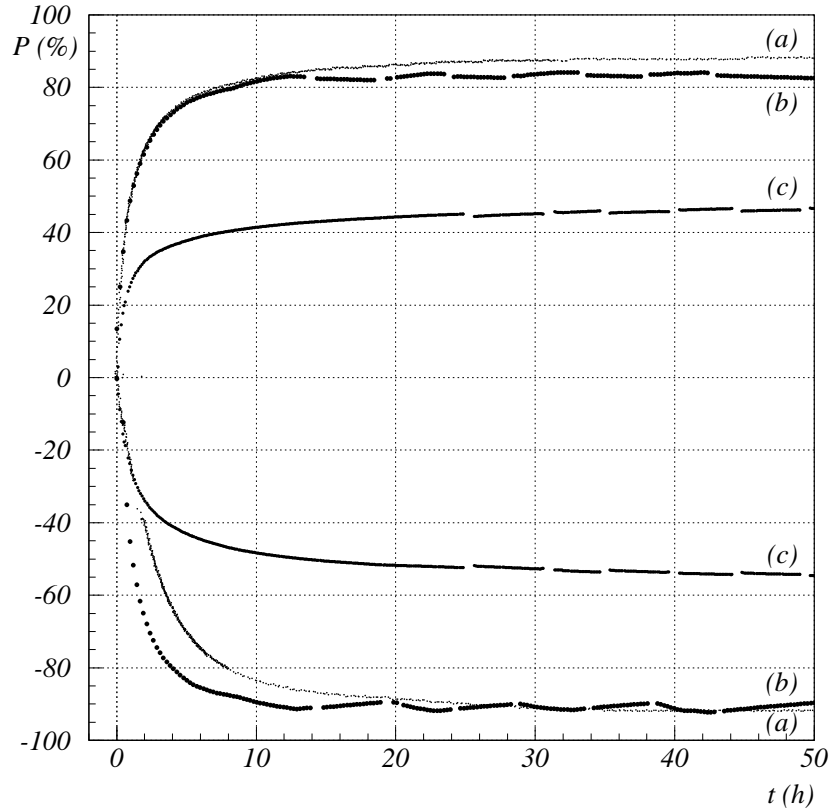


Figure 4: Typical polarization build-up in the target materials, (a) ammonia, (b) butanol, and (c) deuterated butanol followed during 50 hours. The breaks in the data sets are interruptions of the measurements due to field rotations.

In this section, we will discuss several problems related to the use of polarized deuterium as an effective neutron target.

4.1 Spin asymmetries for a polarized deuteron.

Since the deuteron has spin one, 3 states with spin projections +1, 0 and -1 on the reference axis have to be considered. The **vector polarization** P is defined as the difference between the number of deuterons with spin projections +1 and -1 by the total :

$$P = \frac{n_+ - n_-}{n_+ + n_- + n_0}. \quad (27)$$

The number of interactions in 2 target cells ("u" and "d") with polarization anti-parallel and parallel to the beam polarization will be given by

$$\begin{aligned} N_u &= \phi a_u (n_+ \sigma^{\leftarrow\Rightarrow} + n_- \sigma^{\leftarrow\Leftarrow} + n_0 \sigma^{\leftarrow 0}) \\ N_d &= \phi a_d (n_- \sigma^{\leftarrow\Rightarrow} + n_+ \sigma^{\leftarrow\Leftarrow} + n_0 \sigma^{\leftarrow 0}). \end{aligned} \quad (28)$$

For simplicity we assume here $a_u = a_d = 1$, so that the counting rate asymmetry $\delta = (N_u - N_d)/(N_u + N_d)$ becomes

$$\delta = \frac{(n_+ - n_-)(\sigma^{\leftarrow\Rightarrow} - \sigma^{\leftarrow\Leftarrow})}{(n_+ + n_-)(\sigma^{\leftarrow\Rightarrow} + \sigma^{\leftarrow\Leftarrow}) + 2n_0 \sigma^{\leftarrow 0}}. \quad (29)$$

If in addition we assume that the **tensor asymmetry** is zero, the 3 spin cross sections are related by

$$2 \sigma^{\leftarrow 0} = \sigma^{\leftarrow\Rightarrow} + \sigma^{\leftarrow\Leftarrow} \quad (30)$$

and the counting rate asymmetry reduces to

$$\delta = P \frac{\Delta\sigma}{2\bar{\sigma}} = P A_{\parallel}, \quad (31)$$

i.e. to the same relation as for spin 1/2 particles. The formalism developed in the previous sections for the proton remains thus fully applicable to the deuteron, with the only restriction that the polarization (Eqn.27) is defined in a different way. This different definition explains the lower values reached in the build-up of the deuterated butanol polarization as shown by curve (c) on Fig. 4.

4.2 Deuteron spin and nucleon spin.

When the deuteron is in a S state, it is obvious that the proton and the neutron spin are aligned with the deuteron spin, i.e. both nucleon spin projections are +1/2 when the deuteron spin projection is +1. The situation is more complicated when the deuteron is in D state, since the L = 2 angular momentum has to be combined with the nucleon spins [11]. As an example, the deuteron state $|J, J_Z \rangle = |1, 1 \rangle$ is obtained from the following combination of orbital momentum $|L, L_Z \rangle$ and total nucleon spin $|S, S_Z \rangle$:

$$|1, 1 \rangle = \sqrt{3/5} |2, 2 \rangle - |1, -1 \rangle - \sqrt{3/10} |2, 1 \rangle - |1, 0 \rangle + \sqrt{1/10} |2, 0 \rangle - |1, 1 \rangle. \quad (32)$$

There is thus a probability of 3/5 to have both nucleon spins opposed to the deuteron spin, a probability of 3/10 to have one of the nucleon spins aligned with the deuteron spin and the other one in the opposite direction and a probability of 1/10 to have the 2 nucleon spins aligned with the deuteron spin. In total, when the deuteron is in D state, the probability to have one of the nucleon spins opposed to the deuteron spin is 0.75. The D state probability itself ω_d is of the order of 6 % in all models of the deuteron.

Defining an "average nucleon N " with $\sigma_N = (\sigma_p + \sigma_n)/2$, we obtain the following relation between the deuteron and nucleon spin cross sections:

$$\begin{aligned}\sigma_d^{\leftarrow\Rightarrow} &= (1 - 0.75 \omega_d) \sigma_N^{\leftarrow\Rightarrow} + 0.75 \omega_d \sigma_N^{\leftarrow\leftarrow} \\ \sigma_d^{\leftarrow\leftarrow} &= (1 - 0.75 \omega_d) \sigma_N^{\leftarrow\leftarrow} + 0.75 \omega_d \sigma_N^{\leftarrow\Rightarrow}.\end{aligned}\quad (33)$$

The difference between these 2 relations yields

$$g_1^d(x) = (1/2) (1 - 1.5 \omega_d) (g_1^p(x) + g_1^n(x)). \quad (34)$$

4.3 Deuteron and nucleon spin asymmetries.

The deuteron spin asymmetry

$$A_{\parallel}^d = (1 - 1.5 \omega_d) \frac{\Delta\sigma_N}{2\bar{\sigma}_N} \quad (35)$$

can be split into a proton and a neutron term:

$$A_{\parallel}^d = (1 - 1.5 \omega_d) \left[\frac{\Delta\sigma_p}{2\bar{\sigma}_p} \frac{\bar{\sigma}_p}{\bar{\sigma}_N} + \frac{\Delta\sigma_n}{2\bar{\sigma}_n} \frac{\bar{\sigma}_n}{\bar{\sigma}_N} \right]. \quad (36)$$

Replacing the ratios of cross sections by the corresponding ratios of F_2 's and taking out the virtual photon depolarization factor one obtains:

$$A_{\parallel}^d(x) = \frac{(1 - 1.5 \omega_d)}{1 + F_2^n(x)/F_2^p(x)} \left(A_{\parallel}^p(x) + \frac{F_2^n(x)}{F_2^p(x)} A_{\parallel}^n(x) \right), \quad (37)$$

which is the basic relation to extract neutron asymmetries from deuteron data and from previously measured proton asymmetries. The ratio $F_2^n(x)/F_2^p(x)$ has been measured with great precision in several unpolarized experiments [12, 13] and decreases rapidly for $x \geq 0.05$ (Fig. 5).

As a consequence, deuteron data at larger x give relatively little information about the neutron asymmetry. It is only at very low x (≤ 0.01) that A_{\parallel}^d can be considered in first approximation as the average of the proton and neutron asymmetries.

5 Unpolarized material in polarized targets.

The fraction of "useful" (polarizable) material in a polarized target can be evaluated in very first approximation by the ratio of the number of polarizable nucleons to the total number: 3/17 for NH_3 , 10/74 for butanol ($\text{C}_4\text{H}_9\text{OH}$), 20/84 for deuterated butanol ($\text{C}_4\text{D}_9\text{OD}$) and 4/8 for deuterated lithium (LiD) when Li is considered as ($\text{He}^4 + \text{D}$). However, a much more detailed evaluation is needed for 2 reasons:

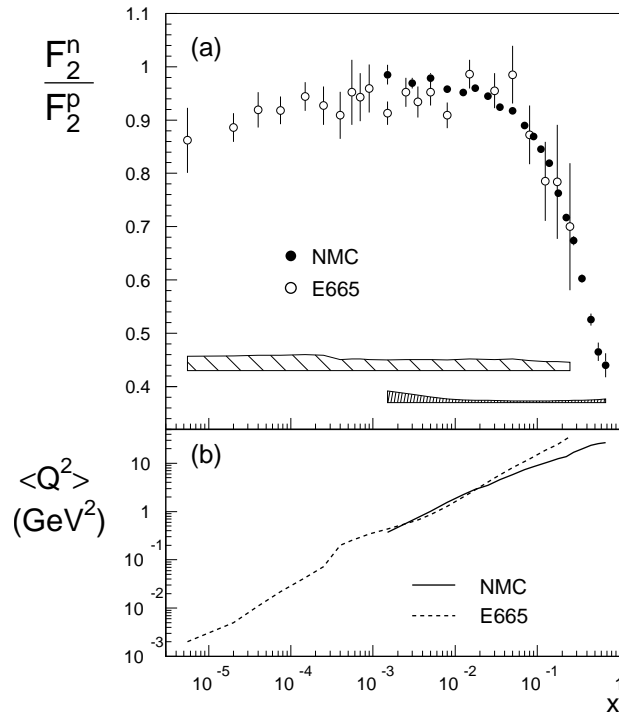


Figure 5: (a) Comparison of the x dependence of the NMC data for F_2^n/F_2^p with the results from the experiment E665 [13]. The error bars correspond to the statistical errors, the shaded bands to the systematic errors. (b) Average Q^2 of the 2 data sets as a function of x .

- **all elements** of the target have to be taken into account, including impurities in the target material, target windows, cooling mixture and coils used for the measurement of the polarization if they are embedded in the material;
- **the number of nucleons** in the ratios must be weighted by the respective cross sections.

We will only discuss here the second point, which has some general implications related to lepton-nucleon interactions and will assume, for clarity, that we are dealing with a proton target ("H").

In general, the dilution factor is defined as

$$f(x) = \frac{n_H \bar{\sigma}_H^T}{\sum_A n_A \bar{\sigma}_{N(A)}^T} \quad (38)$$

where the index "T" refers to total cross sections (including radiative effects). In this formula, n_A is the total number of nucleons (for the full target) in nuclei with atomic

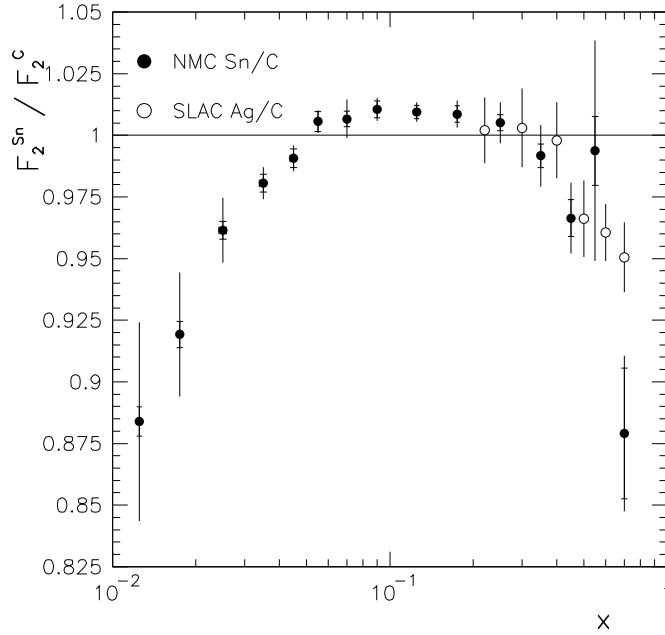


Figure 6: *Structure function ratios for thin and carbon as a function of x , averaged over Q^2 [16]. The inner error bars represent the statistical uncertainty, the outer errors the statistical and systematic uncertainties added in quadrature. The normalisation error is 0.2% and is not included in the systematic uncertainty. The SLAC-E139 [17] ratios for silver and carbon are also plotted (open points).*

number A and $\bar{\sigma}_{N(A)}$ the unpolarized cross section **per nucleon** on nucleus A . Weighting by cross sections is essential because the cross section on a nucleon bound in a nucleus differs from the cross section on a free nucleon. The ratio

$$\bar{\sigma}_{N(C)}/\bar{\sigma}_N \simeq F_2^C(x, Q^2)/F_2^N(x, Q^2) \quad (39)$$

has been measured with high precision over wide ranges of x and Q^2 [14]. Extensive studies have also been performed for a large choice of other nuclei (for a review, see [15]). The ratios $F_2^A/F_2^C = (F_2^A/F_2^N)/(F_2^C/F_2^N)$ always present a very characteristic dependence on x , as illustrated in Fig. 6 for Sn and Ag.

In the very small x region, the cross section on a bound nucleon is reduced with respect to the cross section on a free nucleon. This effect, known as "shadowing" becomes

more pronounced for heavier nuclei. Its name originates from a geometrical interpretation where nucleons inside the nucleus are assumed to be screened by those at the outer surface, resulting in a total cross section proportionnal to $A^{2/3}$ rather than to A . At slightly larger x ($0.05 \leq x \leq 0.2$), the cross section on a bound nucleon is slightly larger than on a free nucleon, while, for $x \geq 0.3$, the ratio (39) drops again due to the so-called "EMC effect" [18].

Measured cross section ratios with respect to C or D exist for a large number of nuclei. For the remaining ones, the ratio at a given x can be approximated by an interpolation as a function of A as shown in Fig. 7 [19].

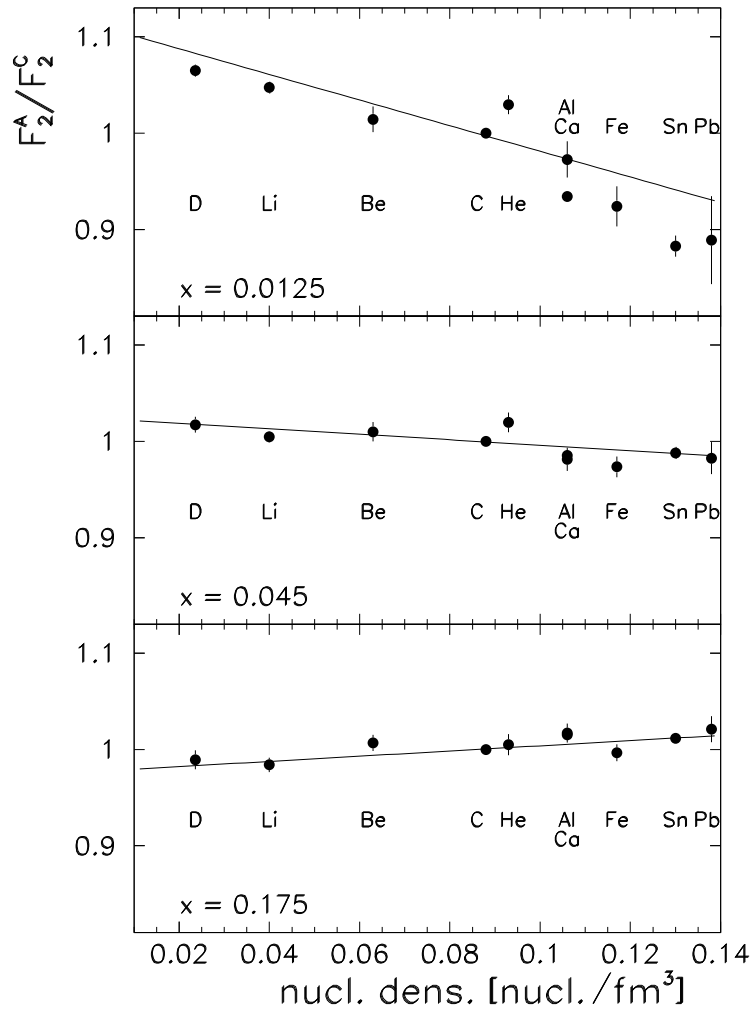


Figure 7: *Structure function ratios measured by the NMC versus nuclear density ρ at $x = 0.0125$, $x = 0.045$ and $x = 0.175$ [19]. The solid lines show the result of a fit to the data with the function $F_2^A/F_2^C = \beta + \delta\rho(A)$. The errors shown are statistical only.*

The resulting dilution factor is shown in Fig. 8 as a function of x for the 3 targets used in the SMC experiment. All curves show a significant drop at low x due to the large

radiative cross sections on nuclei in this region. The rise observed at large x for NH_3 and p-butanol results from the drop of the ratio F_2^n/F_2^p discussed in the previous section.

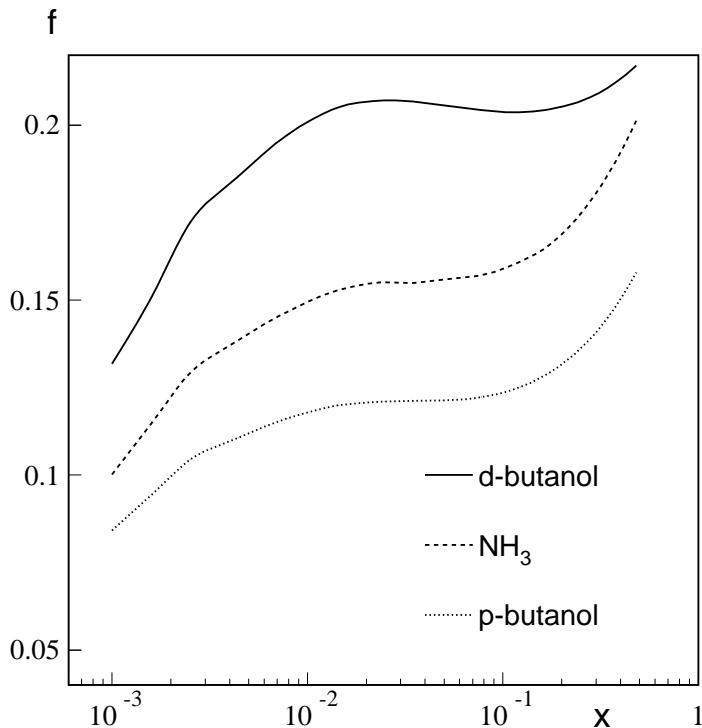


Figure 8: *The dilution factors f for the different target materials used in the SMC experiment as function of Bjorken x . The curves (from top to bottom) correspond to deuterated butanol, ammonia and butanol.*

A further correction is needed when the diluting material itself contains some polarizable nuclei as for instance ^{14}N in the SMC ammonia target [7]. Several other cases (not mentioned here) are discussed in ref. [11].

In addition to dilution due to the presence of non-polarized material in the target, one has to take into account an additional effect due to radiative events taking place on the polarized proton or deuteron. These radiative contributions modify both the spin-averaged and spin dependent cross sections with respect to the value expected from the one photon exchange process (Fig. 1). In general the total (one-photon exchange + radiative processes) cross sections σ^T and the one-photon exchange $\sigma^{1\gamma}$ cross sections are related by

$$\begin{aligned}\bar{\sigma}^T &= v \bar{\sigma}^{1\gamma} + \bar{\sigma}_{tail} \\ \Delta\sigma^T &= v \Delta\sigma^{1\gamma} + \Delta\sigma_{tail}.\end{aligned}\tag{40}$$

The factor v is very close to 1 and will not be further mentioned. The "tail" terms contain contributions from radiative corrections to elastic scattering (with final state $\ell N \gamma$) and from the inelastic continuum. These contributions have been calculated in great detail for the spin averaged and the spin dependent cross sections and can be obtained from specialized computer codes [20]. The measured asymmetry

$$A_{meas} = P_b P_T f \frac{\Delta\sigma^T}{2\bar{\sigma}^T} \quad (41)$$

can be rewritten as

$$A_{meas} = P_b P_T f' \frac{\bar{\sigma}^{1\gamma}}{\bar{\sigma}^T} \frac{\Delta\sigma^T}{2\bar{\sigma}^{1\gamma}} \quad (42)$$

where it appears that

$$f' = f \frac{\bar{\sigma}^{1\gamma}}{\bar{\sigma}^T} \quad (43)$$

is the "effective dilution factor" taking into account radiative effects. This leads to the relation

$$A_{meas} = P_B P_T f' \left(\frac{\Delta\sigma^{1\gamma}}{2\bar{\sigma}^{1\gamma}} + \frac{\Delta\sigma^{tail}}{2\bar{\sigma}^{1\gamma}} \right) \quad (44)$$

where the asymmetry is split into 2 terms corresponding respectively to pure one-photon exchange and to radiative effects. In the usual kinematic conditions, the second term represents a rather small correction (less than 10 % of the one-photon term). In contrast, the change in the dilution factor (f' compared to f) becomes a major effect at small x : for $Q^2 \simeq 1 \text{ GeV}^2$ and $x = 0.005$, the ratio f'/f is of the order of 0.66.

This feature makes asymmetry measurements very unaccurate at low x , except if a large fraction of the radiative events can be eliminated from the data set. This can be achieved by selecting events with at least one high-energy hadron in the final state (e.g. by use of a calorimeter). In this way, the radiative effects due to the elastic tail do not contribute any more and the effective dilution factor no longer drops at low x . The effect of selecting hadron-tagged events is illustrated in Fig. 9 for the ammonia target in the SMC experiment [21].

6 Evaluation of sum rules.

In the previous sections, we have shown how the longitudinal spin structure function $g_1(x, Q^2)$ can be evaluated in the range of x covered by an experiment. The evaluation of the first moment $\Gamma_1(Q_0^2) = \int_0^1 g_1(x, Q_0^2) dx$ involves also the unmeasured range of x and is thus not a fully measurable quantity. Splitting the integration over the measured and unmeasured range of x one obtains

$$\Gamma_1(Q_0^2) = \int_0^{x_{min}} g_1(x, Q_0^2) dx + \int_{x_{min}}^{x_{max}} g_1(x, Q_0^2) dx + \int_{x_{max}}^1 g_1(x, Q_0^2) dx. \quad (45)$$

The contribution of the last term is limited by the boundary condition $|A_1| \leq 1$ and by the small value of the unpolarized structure function F_2 at large x and is thus not critical.

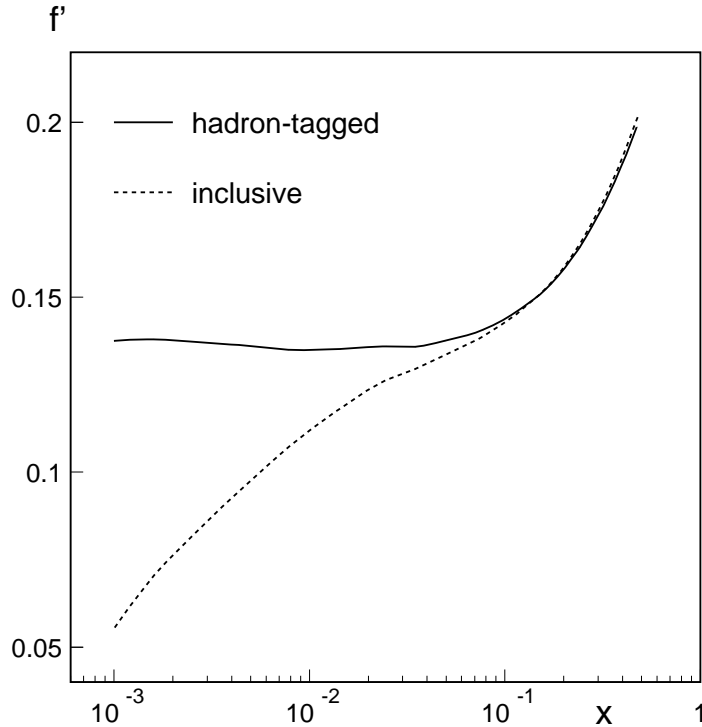


Figure 9: *Effective dilution factor f' for hadron tagged and inclusive events from the SMC ammonia target.*

In contrast, the unmeasured contribution at low x may be important and may influence significantly sum rules involving Γ_1 .

The value of x_{min} depends on the experiment kinematics and on the choice of Q_0^2 :

$$x_{min}(Q_0^2) = \frac{Q_0^2}{2 M \nu_{max}} = \frac{Q_0^2}{2 M y_{max} E_{beam}}. \quad (46)$$

Requiring $Q_0^2 = 1\text{GeV}^2$ to remain in the DIS region and setting $y_{max} = 0.9$, we obtain $x_{min} = 0.003$ for a beam energy of 200 GeV. This is indeed the lowest experimental value of x reached up to now for $Q^2 \geq 1 \text{ GeV}^2$. The integral of $g_1(x)$ below this value can, in principle, be estimated by a smooth extrapolation of the values obtained at higher x taking into account the known asymptotic behaviour of cross sections at high energy. An extrapolation of this kind is shown by the dot-dashed line in Fig. 10 for the SMC data on g_1^p . There is however an ambiguity in this procedure since the experimental values of g_1 are obtained at a different Q^2 for each x interval and need to be evolved to a common (and arbitrary) Q^2 before any extrapolation can be performed. For this reason, a different procedure has been adopted in the most recent evaluations of sum rules.

The analysis of the Q^2 dependence of $g_1(x, Q^2)$ requires input parametrizations of the constituent spin distributions $\Delta q_i(x, Q_0^2)$ at a reference Q^2 value which is most frequently

chosen to be 1 GeV^2 . These parametrizations are then evolved according to the evolution equations of QCD and adjusted to the experimental values of g_1 . The curves on Fig. 3 show that they provide a satisfactory description of the data. In view of this, one may assume that the same parametrizations remain valid below the lowest x value of the measurements and use the fitted g_1 distribution to evaluate the unmeasured contribution at low x . The continuous line in Fig. 10 shows that this approach leads to a very different result compared to the "smooth extrapolation" described before: $g_1(x)$ becomes negative below 0.001, i.e. slightly below the lowest data point. This affects significantly the first moments of g_1 as well for the proton as for the deuteron. The values obtained in the measured range and the estimated low x contributions at $Q^2 = 10 \text{ GeV}^2$ are shown in Table 1 for the SMC experiment.

	Measured range 0.003 - 0.7	Extrapolation 0.0 - 0.003
Γ_1^p	0.131 ± 0.009	-0.011
Γ_1^d	0.037 ± 0.007	-0.018

Table 1: *Low x extrapolation of g_1^p and g_1^d in the SMC experiment at $Q^2 = 10 \text{ GeV}^2$ [21].*

7 Prospects and future experiments.

In the previous sections we have shown how the longitudinal spin structure function has been measured in several polarized DIS experiments over the last 20 years. The precision of the results is limited by the statistical accuracy of the data and their range is limited by the kinematics of fixed target experiments. There are also further limitations inherent to the physics of inclusive reactions: the structure function g_1 does not fully describe the distribution of the nucleon spin. In particular it provides little discrimination between quark flavors and no discrimination at all between quarks and antiquarks.

Additional information can be obtained by studying semi-inclusive reactions, i.e. by requiring the presence of a given hadron in the final state. This can only be achieved in an experiment providing particle identification. Detailed studies of semi-inclusive polarized scattering are presently under way in the HERMES experiment.

The gluon spin distribution Δg contributes to g_1 only by the Q^2 evolution and is therefore poorly constrained by inclusive measurements. A more direct determination of Δg can be achieved by selecting final states mainly produced by the interaction of a gluon with the exchanged virtual photon. This is the case in particular for the production of charmed quarks ($\gamma^* g \rightarrow c\bar{c}$), a process presently studied by the COMPASS experiment at CERN [23].

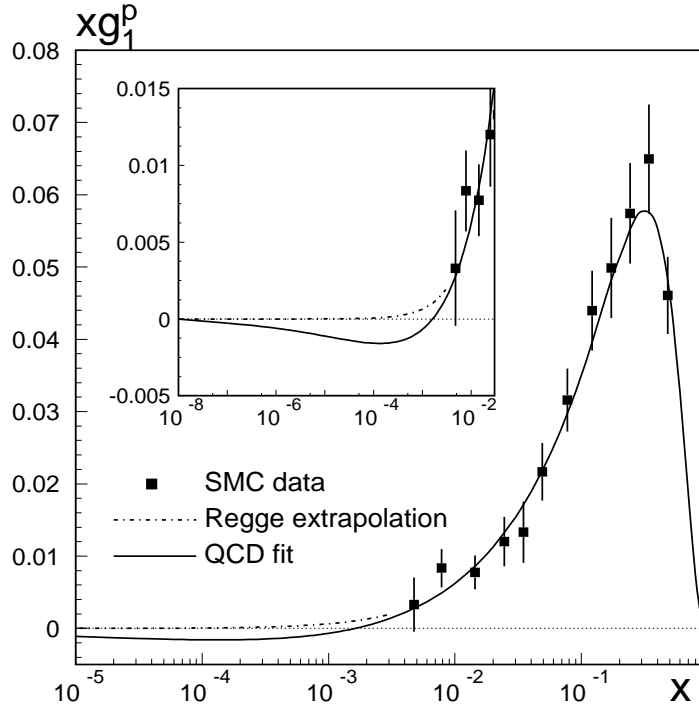


Figure 10: xg_1^p as a function of x ; SMC data points (squares) with the total error are shown together with the result of the QCD fit (continuous line), both at $Q^2 = 10 \text{ GeV}^2$. For $x < 0.003$ the extrapolation assuming Regge behaviour is indicated by the dot-dashed line. The inlet is a close-up extending to lower x . [22]

In addition to g_1 , another structure function, the so-called transversity distribution, can be measured in reactions where the polarization of the target nucleons is perpendicular to the beam polarization [24]. This function is related to the transverse spin distribution of the quarks in the same way as g_1 is related to their longitudinal spin distribution. Transversity will also be measured by the HERMES and COMPASS experiments.

The possibility to extend the kinematic domain of polarized DIS scattering has been investigated by different study groups over the last five years. Projects have been developed for a polarized proton ring at HERA [25] and for an electron-ion collider at BNL [26]. In both projects, the lower limit of x would be considerably reduced and negative values of g_1^p would become observable if the presently used extrapolation is correct.

References

- [1] P.Renton, "Electroweak Interactions, an introduction to the physics of quarks and leptons", Cambridge University Press, 1990 (pp. 318-324).
- [2] G.Baum et al., Phys. Rev. Lett. 51 (1983) 1135.
- [3] CLAS Collab., R. De Vita et al., "First Measurement of the Double Spin Asymmetry in $e p \rightarrow e' \pi^+ n$ in the Resonance Region", hep-ex/0111074 (7 Feb. 2002).
- [4] SLAC-E155 Collab., P.L. Anthony et al., Phys. Lett. B493 (2000) 19; G. Peterson, "Gluon Spin Distributions and GDH Sum rule Measurements at SLAC", Proc. of the IX Int. Workshop on Deep Inelastic Scattering, Bologna, 27 April - 1 May 2001.
- [5] HERMES Collab., K.Ackerstaff et al., Phys. Lett. B404 (1997) 383; A. Airapetian et al. B442 (1998) 484.
- [6] SMC, D.Adams et al., Nucl. Instr. & Meth., A 443 (2000) 1.
- [7] SMC, D.Adams et al., Nucl. Instr. & Meth., A 437 (1999) 23.
- [8] SMC, B.Adeva et al., Phys. Rev. D58 (1998) 112002.
- [9] SMC, D.Adams et al., Phys. Rev.D56 (1997) 5330.
- [10] EMC, C.Caputo and R.Piegaia, "Some Considerations on the Extraction of Asymmetries from the Polarized Target Data and the Inclusion of the Acceptance Correction", internal report EMC/86/5.
- [11] O.A. Rondon, Phys. Rev. C60 (1999) 035201.
- [12] NMC, M.Arneodo et al., Nucl. Phys. B487 (1997) 3.
- [13] E665, M.R. Adams et al., Z. Phys. C 67 (1995) 403.
- [14] M.Arneodo et al., Nucl. Phys. B441 (1995) 12.
- [15] M.Arneodo, Phys. Rep. 240 (1994) 301.
- [16] NMC, M.Arneodo et al., Nucl. Phys. B481 (1996) 23.
- [17] SLAC-E139, R.G.Arnold et al., Phys. Rev. Lett. 52 (1984) 727.
- [18] T.Sloan, G.Smadja and R.Voss, Phys. Rep. 162 (1988) 45.
- [19] NMC, M.Arneodo et al., Nucl. Phys. B481 (1996) 3.
- [20] T.V.Kukhto and N.M.Shumeiko, Nucl. Phys. B219 (1983) 412; I.V.Akushevich and N.M.Shumeiko, J.Phys. G20 (1994) 513.

- [21] SMC, B.Adeva et al., Phys. Rev. D58 (1998) 112001.
- [22] SMC, B.Adeva et al., Phys. Lett. B412 (1997) 414-424.
- [23] G.K.Mallot, "Spin Physics with COMPASS", Proc. of the 12th Int. Symp. on High Energy Physics, Amsterdam 1996 (pp.441-445).
- [24] X.Artru, J.Czyzewski and H.Yabuki, Z. Phys. C 73 (1997) 527.
- [25] "Polarized Protons at High Energies - Accelerator Challenges and Physics Opportunities", DESY-PROC-1999-03 (Ed. by A. De Roeck, D.Barber and G.Rädel).
- [26] <http://www.bnl/eic>